Animal Nutrition 18 (2024) 450–463

Contents lists available at ScienceDirect

Animal Nutrition

journal homepage: http://www.keaipublishing.com/en/journals/aninu/

Original Research Article

Establishing the link between D-mannose and juvenile grass carp (*Ctenopharyngodon idella*): Improved growth and intestinal structure associated with endoplasmic reticulum stress, mitophagy, and apical junctional complexes

Chong Zhang [a], Lin Feng [a, b, c], Pei Wu [a, b, c], Yang Liu [a, b, c], Xiaowan Jin [a], Hongmei Ren [a], Hua Li [a], Fali Wu [a], Xiaoqiu Zhou [a, b, c, *], Weidan Jiang [a, b, c, *]

[a] *Animal Nutrition Institute, Sichuan Agricultural University, Chengdu 611130, China*
[b] *Fish Nutrition and Safety Production, University Key Laboratory of Sichuan Province, Sichuan Agricultural University, Chengdu 611130, China*
[c] *Key Laboratory of Animal Disease-Resistance Nutrition, Ministry of Education, Ministry of Agriculture and Rural Affairs, Key Laboratory of Sichuan Province, Chengdu 611130, China*

ARTICLE INFO

Article history:
Received 8 January 2024
Received in revised form
21 February 2024
Accepted 6 May 2024
Available online 29 June 2024

Keywords:
Grass carp (*Ctenopharyngodon idella*)
D-mannose
Intestine structure
Endoplasmic reticulum stress
Mitophagy
Apical junctional complex

ABSTRACT

D-mannose, essential for protein glycosylation, has been reported to have immunomodulatory effects and to maintain intestinal flora homeostasis. In addition to evaluating growth performance, we examined the impact of D-mannose on the structure of epithelial cells and apical junction complexes in the animal intestine. All 1800 grass carp (16.20 ± 0.01 g) were randomly divided into six treatments with six replicates of 50 fish each and fed with six different levels of D-mannose (0.52, 1.75, 3.02, 4.28, 5.50 and 6.78 g/kg diet) for 70 d. The study revealed that D-mannose increased feed intake ($P < 0.001$) but did not affect the percent weight gain (PWG), special growth rate, and feed conversion ratio ($P > 0.05$). D-mannose supplementation at 1.75 g/kg increased crude protein content in fish and lipid production value ($P < 0.05$). D-mannose supplementation at 4.28 g/kg increased intestinal length, intestinal weight and fold height of grass carp compared to the control group ($P < 0.05$). This improvement may be attributed to the phosphomannose isomerase (PMI)-mediated enhancement of glycolysis. This study found that D-mannose supplementation at 4.28 or 3.02 g/kg reduced serum diamine oxidase activity or D-lactate content ($P < 0.05$) and improved cellular and intercellular structures for the first time. The improvement of cellular redox homeostasis involves alleviating endoplasmic reticulum (ER) stress through the inositol-requiring enzyme 1 (IRE1), RNA-dependent protein kinase-like ER kinase (PERK), and activating transcription factor 6 (ATF6) signaling pathways. The alleviation of ER stress may be linked to the phosphomannomutase (PMM)-mediated enhancement of protein glycosylation. In addition, ubiquitin-dependent [PTEN-induced putative kinase 1 (PINK1)/Parkin] and ubiquitin-independent [BCL2-interacting protein 3-like (BNIP3L), BCL2-interacting protein 3 (BNIP3), and FUN14 domain containing 1 (FUNDC1)] mitophagy may play a role in maintaining cellular redox homeostasis. The enhancement of intercellular structures includes enhancing tight junction and adherent junction structures, which may be closely associated with the small Rho GTPase protein (RhoA)/the Rho-associated protein kinase (ROCK) signaling pathway. In conclusion, D-mannose improved intestinal cellular redox homeostasis associated with ER stress and mitophagy pathways, and enhanced intercellular structures related to tight junctions and adherent junctions. Furthermore, quadratic regression analysis of the PWG and intestinal

Peer review under responsibility of Chinese Association of Animal Science and Veterinary Medicine.

Production and Hosting by Elsevier on behalf of KeAi

* Corresponding authors.
E-mail addresses: zhouxq@sicau.edu.cn (X. Zhou), WDJiang@sicau.edu.cn (W. Jiang).

https://doi.org/10.1016/j.aninu.2024.05.003

reactive oxygen species content indicated that the optimal addition level of D-mannose for juvenile grass carp was 4.61 and 4.59 g/kg, respectively.

1. Introduction

The intestinal structure is of paramount importance for the healthy growth of fish (Pang et al., 2023). However, the increasing intensification of aquaculture has made the gut more vulnerable to external stresses, such as pathogens (Aly et al., 2024). The study demonstrated that mannan oligosaccharides could safeguard the gut health of fish (Lu et al., 2020). D-mannose, a C-2 epimer of glucose, plays a crucial role in protein glycosylation (Loke et al., 2016) and is widely recognized as a popular nutritional and healthful food supplement globally (Ichikawa et al., 2014). D-mannose is widely distributed in the animal organism, particularly in the intestine (Wei et al., 2020). D-mannose was reported to maintain intestinal flora homeostasis and have immunomodulatory effects in mice (Xiao et al., 2022). A study showed that D-mannose reduced weight loss in mice with experimental colitis (Dong et al., 2022). Nevertheless, the impact of D-mannose on the intestinal structure in fish has not been reported yet. D-mannose was transported into intestinal epithelial cells primarily through glucose transporters (Tazawa et al., 2005) and alleviated intestinal structural damage in mice (Xiao et al., 2022). These results suggest that D-mannose might enhance intestinal structure, but additional research is required.

The structural integrity of the animal gut is closely linked to the redox homeostasis of the organism (Homolak et al., 2021). Redox homeostasis in organisms relies on the participation of the endoplasmic reticulum (ER) and mitochondria (Babaei-Abraki et al., 2022). Endoplasmic reticulum stress induces the unfolded protein response (UPR), in which the glucose-regulated protein 78 (GRP78) and C/EBP homologous protein (CHOP) play a crucial role (Hetz, 2012). Mitophagy is primarily controlled by the PTEN-induced putative kinase 1 (PINK1)/Parkin pathway and receptor-mediated pathways, playing a crucial role in maintaining mitochondrial quality (Palikaras et al., 2018). A study showed that D-mannose reduced oxidative stress in neuroinflammatory mice (Wang et al., 2021c). However, there is a lack of research on how D-mannose affects the structure of intestinal cells and related signaling in fish. D-mannose has been found to increase intestinal butyrate levels in zebrafish (Wang et al., 2021a). Sodium butyrate decreased *CHOP* expression to alleviate ER stress in mice (Kushwaha et al., 2022). D-mannose was found to activate 5′ AMP-activated protein kinase (AMPK) in interleukin-1β (IL-1β)-induced rat chondrocytes (Lin et al., 2021). The AMPK activation mediates mitophagy through the PINK1/Parkin-mediated pathway (Cao et al., 2021). Thus, D-mannose likely affects intestinal epithelial cells by regulating ER stress and mitophagy. However, additional research is necessary to confirm this.

In addition, the structural integrity of the intestine also depends on intercellular structures. The intercellular structures primarily comprise the apical junctional complex (AJC), consisting of the tight junction (TJ) and adherent junction (AJ) (Adil et al., 2021). The maintenance of AJC is regulated by myosin light chain kinase (MLCK) through the small Rho GTPase protein (RhoA)/the Rho-associated protein kinase (ROCK) pathway (Jin and Blikslager, 2020). However, it has not been reported whether D-mannose could influence the intestinal AJC structure and related pathways in animals. D-mannose inhibited IL-1β secretion in mouse macrophages (Torretta et al., 2020). In Caco-2 cells, the reduced IL-1β inhibited *MLCK* expression and decreased intestinal epithelial cell permeability (Al-Sadi et al., 2010). D-mannose was found to inhibit the extracellular signal-regulated kinase (ERK) pathway in A549 cells (Wang et al., 2020). The ERK pathway regulates RhoA activity in colon carcinoma cells (Vial et al., 2003). These results lead us to believe that D-mannose might influence the structure of the fish gut AJC and associated pathways, but this hypothesis requires further testing.

Grass carp are the most productive freshwater fish globally (Xu et al., 2021). With increasing intensification, key focus areas for aquaculture transformation in Asia include the utilization of innovative feed additives (FAO, 2022). As far as we know, the optimal level of D-mannose addition has only been reported in one article on the model animal, zebrafish. A study showed that D-mannose improved zebrafish health, with the optimal level being 5 g/kg (Wang et al., 2021a). Accordingly, there is a significant need to conduct studies on the optimal levels of D-mannose in economically farmed fish, such as grass carp (*Ctenopharyngodon idellus*).

Conclusively, we also investigated the effects of D-mannose on the cell structure and AJC in the animal intestinal epithelium, which involves ER stress, mitophagy, and RhoA/ROCK-related signaling pathways for the first time. Our findings may serve as a partial theoretical basis for investigating the function and mechanism of D-mannose on animal gut health. We further determined the optimal level of D-mannose addition in grass carp, which may provide guidance for enhancing fish performance and feed formulation.

2. Materials and methods

2.1. Animal ethics statement

The Animal Care Advisory Committee of Sichuan Agricultural University supported the entire procedure of this experiment (No. ZC-2021214059).

2.2. Experimental designs

Table 1 represents the composition and nutrient levels of the basal diet in this trial. The experiment utilized fish meal, soybean protein isolate, cottonseed meal, and rapeseed meal as protein sources, in addition to fish oil and soybean oil as lipid sources. The diets were formulated to be isonitrogenous and isolipidic. The D-mannose (99% purity, Feed Research Institute, Chinese Academy of Agricultural Sciences, Beijing, China) was added at 0, 1.25, 2.50, 3.75, 5.00, and 6.25 g/kg diet to formulate the test diets, with the remainder compensated by microcrystalline cellulose. Research has shown that D-mannose is not well metabolized to provide energy in the body, and most of the D-mannose that enters the body is excreted in the urine within 1 h (Scaglione et al., 2021). It acts like dietary fiber, so the grade levels of D-mannose are compensated by microcrystalline cellulose. According to Wang et al., 2021a, the final D-mannose contents in six diets were measured to be 0.52, 1.75, 3.02, 4.28, 5.50, and 6.78 g/kg, respectively. First, six different levels of D-mannose were thoroughly mixed with microcrystalline cellulose to prepare D-mannose premixes. Next, the ingredients were

Table 1
Composition and nutrient levels of the basal diet (as-fed basis, g/kg).

Ingredients	Content	Nutrient levels[4]	Content
Fish meal	80.00	Dry matter	893.30
Soybean protein isolate	210.00	Crude protein	310.50
Cottonseed meal	87.30	Crude lipid	45.50
Rapeseed meal	60.00	Ash	70.65
Flour	224.05	n-3 PUFA[5]	10.40
Corn starch	50.00	n-6 PUFA[5]	9.60
Glucose	100.00	Available phosphorus[6]	8.40
Fish oil	22.80		
Soybean oil	8.30		
$Ca(H_2PO_4)_2$	37.90		
Vitamin premix[1]	10.00		
Mineral premix[2]	20.00		
Choline chloride (50%)	10.00		
Butyl hydroxyanisole	0.15		
Carboxymethyl cellulose	20.00		
Triacetin (50%)	0.30		
L-Lys (78.8%)	5.20		
DL-Met (99%)	1.30		
L-Thr (98.5%)	2.70		
D-mannose premix[3]	50.00		
Total	1000.00		

PUFA = polyunsaturated fatty acids.
[1] Per kilogram of vitamin premix (g/kg): retinyl acetate (500,000 IU/g) 0.80, cholecalciferol (500,000 IU/g) 0.32, DL-α-tocopherol acetate (50%) 40.00, menadione (50%) 0.38, thiamine nitrate (98%) 0.16, riboflavin (80%) 0.775, pyridoxine hydrochloride (98%) 0.62, calcium-D-pantothenate (98%) 4.20, niacin (99%) 2.58, meso-inositol (97%) 22.06, cyanocobalamin (1%) 0.94, D-biotin (2%) 1.55, folic acid (95%) 0.38, ascorbic acid (95%) 16.32. All ingredients were diluted with corn starch to 1 kg.
[2] Per kilogram of mineral premix (g/kg): $MnSO_4 \bullet H_2O$ (31.8% Mn) 3.07, $MgSO_4 \bullet H_2O$ (15.0% Mg) 237.83, $FeSO_4 \bullet H_2O$ (30.0% Fe) 12.25, $ZnSO_4 \bullet H_2O$ (34.5% Zn) 7.68, $CuSO_4 \bullet 5H_2O$ (25.0% Cu) 0.95, Ca $(IO_3)_2$ (3.2% I) 1.56, selenium yeast (0.2% Se) 13.65. All ingredients were diluted with corn starch to 1 kg.
[3] D-mannose premix (g/kg diet): provided D-mannose at 0, 1.25, 2.50, 3.75, 5.00, and 6.25 g/kg for the six groups, with the remainder consisting of microcrystalline cellulose. In humans, D-mannose has been found to be poorly metabolized for energy (Scaglione et al., 2021). It acts like dietary fiber, so the grade levels of D-mannose are compensated by microcrystalline cellulose.
[4] Dry matter, crude protein, crude lipid, and ash contents were measured values.
[5] n-3 PUFA and n-6 PUFA contents were referenced to Zeng et al. (2016), and calculated according to NRC (2011).
[6] Available phosphorus was calculated according to NRC (2011).

thoroughly ground using a 300-μm sieve and premixed, after which the oil and water were added. Finally, the diets were well-mixed, processed into pellets, air-dried, and frozen at −20 °C for later use, following the method described by Lu et al. (2020).

2.3. Feeding trial

This experiment was designed with reference to our laboratory's previous methods (Deng et al., 2014). This experiment was conducted at the Ya'an Aquatic Animal Nutrition Experimental Base, Animal Nutrition Institute, Sichuan Agricultural University. After being purchased from the fishery in Deyang, China, grass carp were acclimatized for 1 month under experimental conditions following the method described by Xue et al. (2023). Afterward, 1800 grass carp (16.20 ± 0.01 g) were randomly allocated to 36 square cages with 2.0 m side lengths, each containing 50 fish. The experiment consisted of 6 treatments (6 repetitions per treatment, 50 fish per duplicate). The test fish were fed 4 times daily at 07:00, 11:00, 15:00, and 19:00. Trays (1 m) were placed to allow for the counting of residual feed after a 30-min feeding period, following the method described by Tie et al. (2019). Subsequently, feed intake (FI) was calculated based on the above results. All the cages used in the experiment were placed in outdoor freshwater ponds. To safeguard water quality and maintain dissolved oxygen levels, we conducted daily pond water changes and utilized microporous aeration throughout the test period, following the method outlined by Ma et al. (2023). The experiment lasted 70 d, and a suitable culture environment was maintained (water temperature 23.2 ± 3.8 °C, pH 7.5 ± 0.5, and dissolved oxygen content > 6.0 mg/L). The water quality conditions were determined by averaging the daily measurements of water quality in all ponds. The trial was conducted under natural light conditions.

2.4. Sampling

Fish were fasted for 24 h and weighed after the 70-d test to calculate the final body weight (FBW), percent weight gain (PWG), specific growth rate (SGR), and feed conversion ratio (FCR). We used a 50 mg/L benzocaine bath to euthanize the fish selected randomly, following the procedure described by Yao et al. (2024). Whole fish were sampled to determine their proximate body composition. Before the fish were dissected, indicators such as body weight were first determined. Blood was collected and centrifuged at 3000 × *g* at 4 °C for 10 min to obtain serum, which was used to determine serum diamine oxidase (DAO) activity and D-lactate content following the method described by Yao et al. (2023). Afterward, the hepatopancreas and intestines were rapidly isolated from the fish, weighed, and the intestinal length was measured. Intestines for hematoxylin and eosin (HE) and fluorescent staining were fixed in 4% paraformaldehyde. The intestines were segmented for biochemical and molecular assays, frozen with liquid nitrogen, and then stored at −80 °C, following the method described by Zhang et al. (2019).

2.5. Growth performance

The relevant formulas for growth performance are as follows:

$$\text{PWG}\ (\%) = 100 \times [(\text{FBW, g/fish}) - (\text{IBW, g/fish})]/(\text{IBW, g/fish});$$

$$\text{SGR}\ (\%/\text{d}) = 100 \times [\ln(\text{FBW, g/fish}) - \ln(\text{IBW, g/fish})]/\text{d};$$

$$\text{FCR} = (\text{FI, g/fish})/[(\text{FBW, g/fish}) - (\text{IBW, g/fish})];$$

$$\text{Protein efficiency ratio (PER, \%)} = 100 \times (\text{weight gain, g})/(\text{protein intake, g});$$

$$\text{Protein retention value (PRV, \%)} = 100 \times [(\text{final body protein, g}) - (\text{initial body protein, g})]/(\text{total protein fed, g});$$

$$\text{Lipid production value (LPV, \%)} = 100 \times [(\text{final body lipid, g}) - (\text{initial body lipid, g})]/(\text{total lipid fed, g});$$

$$\text{Hepatosomatic index (HSI, \%)} = 100 \times (\text{wet hepatopancreas weight, g})/(\text{wet body weight, g});$$

$$\text{Intestinal somatic index (ISI, \%)} = 100 \times (\text{intestinal weight, g})/(\text{body weight, g}).$$

2.6. HE staining

Previously fixed intestinal samples were dehydrated, paraffin-embedded, sectioned, rehydrated, and finally stained with HE dye following the standard procedure outlined in Wang et al. (2017). The light microscope (TS100, Nikon, Tokyo, Japan) was used to observe intestinal tissue sections and measure fold height following the method described by Xue et al. (2023).

2.7. Fluorescent staining

The intestinal sections (4 μm) were also deparaffinized and rehydrated according to Roth (2011) before fluorescent staining.

2.7.1. Concanavalin A (ConA) staining

Concanavalin A, a lectin protein obtained from the jack bean, can recognize glycosylated proteins (Qin et al., 2014). After antigen retrieval, the intestinal sections were incubated with fluorescein isothiocyanate (FITC)-labeled ConA stain (Lot#FY66P231223, FeiyuBio, Nantong, China) diluted in 10 μg/mL phosphate-buffered saline (PBS) for 30 min at room temperature.

2.7.2. Thioflavin T (ThT) staining

According to the instructions, intestinal tissue sections were stained using the paraffin section amyloid thioredoxin T fluorescence staining kit (Lot#8-251531-10, GENMED Scientifics Inc., Arlington, MA, USA). After dewaxing and rehydration, the tissue sections were incubated with ThT dye for 10 min at room temperature.

2.7.3. Immunofluorescence

Based on Im et al. (2019), the endogenous enzyme was first inactivated, and then the intestinal sections were heated for antigen retrieval. Primary antibodies, such as GRP78 (A11366), zonula occludens-1 (ZO-1) (A0659), E-cadherin (A11492), and Nectin (A5378) from ABclonal (Wuhan, China), were diluted 1:100 in PBS and incubated overnight at 4 °C after 1 h of blocking. After rinsing with PBS, the intestinal sections were incubated with Alexa Fluor 555-labeled donkey anti-rabbit IgG (Beyotime, Shanghai, China) at room temperature for 1 h, and they were protected from light.

All of them were rinsed and stained with a 4′,6-diamidino-2-phenylindole (DAPI) staining solution for 5 min. After rinsing, a drop of Antifade Mounting Medium (Beyotime, Shanghai, China) was added, and the intestinal slides were sealed with coverslips. Finally, the sections were immediately observed using the inverted fluorescence microscope (DMI4000B; Leica, Oberkochen, Germany). Fluorescence intensity was quantified using ImageJ.

2.8. Biochemical analysis

The diet and whole fish were assayed for proximate composition using routine methods referenced in AOAC (2005). The samples were dried at 105 °C for moisture determination (method 925.10). Crude protein (method 990.03) and crude lipid (method 2003.05) were determined using the Kjeldahl and Soxhlet extraction methods, respectively. Ash (method 923.03) was measured using a muffle furnace at 550 °C. Consistent with the method described by Soyama (1984), the D-mannose content (Lot#G0583W) in both the diet and intestine was determined using the corresponding kit (Grace Biotechnology, Suzhou, China). After the enzyme-catalyzed depletion of endogenous glucose, the level of D-mannose was determined by measuring the increase in nicotinamide adenine dinucleotide phosphate (NADPH) at 340 nm, catalyzed by an enzyme complex that includes hexokinase. The kit (Jiancheng Bioengineering Institute, Nanjing, China) was utilized to measure serum DAO activity (Lot#A088-1-1) based on the depletion rate of nicotinamide adenine dinucleotide (NADH). D-lactate content (Lot#QS48279) was detected using an enzyme-linked immunosorbent assay (ELISA) kit (Jason Bio-Technology Co., Ltd., Beijing, China). A 10% homogenate of the intestinal samples was prepared using 4 °C physiological saline as a solvent and then centrifuged for 20 min (6000 × *g*, 4 °C) to obtain the supernatant. The activities of phosphomannose isomerase (PMI; SMK530492A) and phosphomannomutase (PMM; SMK530488A) were determined using enzyme-linked immunosorbent assay kits from Jiangsu Sumeike Biological Technology Co., Ltd. (Jiangsu, China). The corresponding kits (Jiancheng, Nanjing, China) were used to measure the activities of hexokinase (HK; Lot#A077-3-1), phosphofructokinase (PFK; Lot#A129-1-1), pyruvate kinase (PK; Lot#A076-1-1), and lactate dehydrogenase (LDH; Lot#A020-1-2), as well as lactate levels (LD; Lot#A019-2-1). Using the kit (Beyotime Biotechnology, Shanghai, China), reactive oxygen species (ROS; Lot#S0033S) generation was determined by measuring oxidatively generated 2′,7′-dichlorofluorescein following the method described by LeBel et al. (1992). Meanwhile, redox homeostasis-related indices such as protein carbonyl (PC; Lot#A087-1), malondialdehyde (MDA; Lot#A003-1), and glutathione (GSH; Lot#A006-1-1) content, as well as total antioxidant capacity (T-AOC; Lot#A015-1), superoxide dismutase (SOD; Lot#A001-1), catalase (CAT; Lot#A007-1-1), and glutathione peroxidase (GPx; Lot#A005-1) activities were assayed following the methods outlined by Jiang et al. (2019).

2.9. Real-time qPCR

This method was commonly used in our laboratory for RNA analysis (Xue et al., 2023). We isolated total RNA from fish intestines using the RNAiso Plus kit (Takara, Dalian, China). After measuring RNA quality and purity using 1.5% agarose gel electrophoresis and spectrophotometric analysis, the RNA was reverse transcribed with the PrimeScript RT kit (Takara, Dalian, China). Real-time qPCR was carried out using SYBR Green (Aidlab Biotechnology Ltd.). Specific primers were designed based on grass carp sequences identified in GenBank (Table 2). After screening, β-actin was used as the reference. When the amplification efficiency calculated from the gene-specific standard curve was close to 100%, the $2^{-\Delta\Delta Ct}$ method was used for gene quantification, as described by Livak and Schmittgen (2001).

2.10. Western blot

Similarly, the method commonly used in our laboratory was employed for Western blot analysis (Kuang et al., 2012). Intestinal protein samples were extracted using the relevant kits (Beyotime, Shanghai, China). Protein samples were separated using a 10% sodium dodecyl sulfate-glycine polyacrylamide gel and then transferred to a polyvinylidene difluoride (PVDF) membrane. The facilitative glucose transporter 2 (GLUT2) (A9843, 1:500), Parkin (A0968, 1:1000), the BCL2-interacting protein 3 (BNIP3) (A5683, 1:1000), the FUN14 domain containing 1 (FUNDC1) (A22001, 1:1000), the microtubule-associated protein 1 light chain 3 (MAP1LC3) abbreviated LC3 (A15591, 1:2000), and occludin (A12621, 1:2000) antibodies (ABclonal Technology, Wuhan, China) were incubated with membranes overnight at 4 °C after 2 h of sealing with 5% BSA. Furthermore, glyceraldehyde-3-phosphate dehydrogenase (GAPDH) (A19056, 1:50,000) was used as the control protein. The protein band was blotted using an ECL kit (Beyotime) and analyzed with ImageJ after 2 h of incubation at room temperature with the secondary antibody (AS014, 1:2000) from ABclonal.

2.11. Statistical analysis

Data are presented as means ± standard deviation (SD). Using SPSS 21.0 (SPSS Inc., Chicago, IL, USA), a one-way ANOVA was performed on the acquired data, and Duncan's method was used to determine statistically significant differences between groups ($P < 0.05$). Based on the R^2 and *P*-value of the regression analysis, we selected the appropriate regression model to determine the

Table 2
Real-time qPCR primer sequences.

Gene	Primer sequence forward (5′-3′)	Primer sequence reverse (5′-3′)	Accession number
SGLT4	TTGCTTTGGAGGCTGCAGAT	TGGCTCTGACTGAGGACCAT	XM_051901922.1
GRP78	GTCACCTTTGAGATCGACGTG	AGAGAGTAGGCGTAGCTC	FJ436356
CHOP	ATCAGAACGAGCGCCTCAAA	TTCACCTCCTGGTGTTGACG	KX013389
PERK	CAGCGTTTACCTGGGGATGT	TTACTGCCCCAGGCGTTTAG	KX906957
EIF2A	ATCAATAGCGGAGATGGGCG	TGATGACCACCACGCATTCA	KJ126860
ATF4	TTCGGCCAACACCTTAGACC	CTTGCCTCATCTTTCGGGGT	AY437846
ATF6	CACCTCTGTTCCTGACCTGA	TAGACAGACAGTGGAGAGGG	KT279356
IRE1	GAACGCCACATACTCTGA	TGTCCACTGTCACCACTA	MG797683
XBP1	TTCTGAGTCCGCAGCAGGTG	GTTCTGGGTCAAGGATGTCC	KU509247
PINK1	TGCGGAGACTGAGAAGTG	CCATAGACATAGAGCGAAGGAT	MZ358119
BNIP3L	GCGTTGCTCTTGGTAGATTGC	GGGAGTGGAAAGTTCTGTGGG	Yu et al. (2020)
LC3	ATGCCTTCGGAAAAGACATTTAAAC	TTACTGAGGACACGCAGTTCC	MG821471
P62	TGATGGGGTTGGCTCTTGTGAA	CCTGGAGGGCTAAAGTGGGATG	MK370058
ZO-2b	TACAGCGGGACTCTAAAATGG	TCACACGGTCGTTCTCAAAG	KM112095
JAM	ACTGTGAGGTGCTTGGAA	CTGTTGTGACTGAAGAAGGA	KY780630
Claudin-b	GAGGGAATCTGGATGAGC	ATGGCAATGATGGTGAGA	KF193860
Claudin-c	GAGGGAATCTGGATGAGC	CTGTTATGAAAGCGGCAC	KF193859
Claudin-f	GCTGGAGTTGCCTGTCTTATTC	ACCAATCTCCCTCTTTTGTGTC	KM112097
Claudin-3c	ATCACTCGGGACTTCTA	CAGCAAACCCAATGTAG	KF193858
Claudin-11	TCTCAACTGCTCTGTATCACTGC	TTTCTGGTTCACTTCCGAGG	KT445867
Claudin-12	CCCTGAAGTGCCCACAA	GCGTATGTCACGGGAGAA	KF998571
Claudin-15a	TGCTTTATTTCTTGGCTTTC	CTCGTACAGGGTTGAGGTG	KF193857
Claudin-15b	AGTGTTCTAAGATAGGAGGGGAG	AGCCCTTCTCCGATTTCAT	KT757304
α-catenin	GCAATCTTCTCTCCTTTATCC	ACTTGTGAACTCCAGCAAT	HQ338751
β-catenin	GTCTGCTTGCCATCTTCA	CAGGTTGTGTAGAGTCGTAA	MN661349
Afadin	CCTGTGCTCACACTACTG	GTCGTTGCCTGGACTATG	MN661352
RhoA	GCAGGACAAGAGGACTATG	GTGTTCATCATTCCGTAGGT	MN661351
ROCK	AGTCCAAGTCTGCTGCTA	CCTCTCCTTCTGCTTCATC	KY780630
MLCK	GAAGGTCAGGGCATCTCA	GGGTCGGGCTTATCTACT	KM279719
NMII	AGCCAACTCGTCAATGTC	CCTTGGAATACTTCTCTGTCT	MN661353
β-actin	GGCTGTGCTGTCCCTGTA	GGGCATAACCCTCGTAGAT	M25013

SGLT4 = sodium-glucose linked transporter 4; *GRP78* = glucose regulatory protein 78; *CHOP*=C/EBP homologous protein; *PERK* = protein kinase R-like endoplasmic reticulum kinase; *EIF2A* = eukaryotic initiation factor 2; *ATF4* = activating transcription factor 4; *ATF6* = activating transcription factor 6; *IRE1* = inositol-requiring enzyme 1; *XBP1* = X box-binding protein 1; *PINK1* = PTEN-induced putative kinase 1; *BNIP3L* = BCL2 interacting protein 3-like; *LC3* = light chain 3; *ZO-2b* = zonula occludens-2b; *JAM* = junctional adhesion molecule; *RhoA* = a small Rho GTPase protein; *ROCK* = Rho-associated protein kinase; *MLCK* = myosin light chain kinase; *NMII* = non-muscle myosin II.

optimal addition of D-mannose. Furthermore, Pearson's correlation analyses were conducted.

3. Results

3.1. Influence of D-mannose on growth performance and intestinal development

Table 3 shows that FBW, PWG and SGR were higher in the 4.28 g/kg D-mannose group than in the control group, but there was no significant difference ($P > 0.05$). Feed intake was maximized in the 3.02 g/kg D-mannose group. Compared to the control group, the addition of D-mannose had no significant effect on the FCR ($P > 0.05$). Compared to the control group, there was no significant difference in the survival rate of juvenile grass carp ($P > 0.05$). The protein efficiency ratio and protein retention value did not differ significantly compared to the control group ($P > 0.05$). The lipid production value reached a maximum in the group with 1.75 g/kg of D-mannose. Compared to the control group, the moisture and crude lipid contents of whole fish did not differ significantly ($P > 0.05$). Crude protein content in grass carp reached a maximum in the group with 1.75 g/kg of D-mannose. When D-mannose was added at up to 4.28 g/kg, the ash content in grass carp significantly increased compared to the control group ($P = 0001$). The weight of the hepatopancreas in grass carp significantly increased in the group with 4.28 g/kg of D-mannose compared to the control group ($P < 0.001$). However, there was no significant effect on the hepatosomatic index compared to the control group ($P > 0.05$).

D-mannose supplementation at 4.28 g/kg significantly increased the intestinal length of grass carp compared to the control group ($P = 0.002$). The addition of D-mannose at 4.28 g/kg significantly improved intestinal weight compared to the control group ($P < 0.001$) (Table 3). Figure 1 and Table 4 show that D-mannose supplementation at 4.28 g/kg significantly increased intestinal fold height of grass carp compared to the control group ($P < 0.001$). The addition of D-mannose at 4.28 g/kg significantly increased intestinal D-mannose content compared to the control group ($P < 0.001$) (Table 4). The addition of D-mannose at 4.28 g/kg also significantly increased the mRNA expression level of sodium-glucose linked transporter 4 (*SGLT4*) in fish intestines compared to the control ($P < 0.05$). The addition of 4.28 g/kg D-mannose significantly enhanced intestinal GLUT2 protein expression level compared to the control group ($P < 0.05$) (Fig. 2). As shown in Table 5, D-mannose supplementation at 4.28 g/kg significantly increased intestinal HK, PK, and LDH activities compared to the control group ($P < 0.05$). D-mannose supplementation at 3.02 g/kg significantly reduced intestinal LD content compared to the control group ($P < 0.001$). D-mannose supplementation at 1.75 g/kg in grass carp significantly elevated intestinal PMI activity compared to the control group ($P < 0.001$).

3.2. Influence of D-mannose on intestinal structural integrity

Compared to the control group, D-mannose supplementation at 4.28 g/kg significantly reduced serum DAO activity ($P = 0.001$). The lowest D-lactate content in fish serum was observed with D-mannose supplementation at 3.02 g/kg (Table 4).

3.3. Influence of D-mannose on intestinal redox homeostasis

The addition of D-mannose at 4.28 g/kg significantly reduced the contents of ROS, MDA, and PC in fish intestines compared to the

Table 3
Effects of D-mannose on the growth performance, nutrient conversion rates, whole-body nutritional components and morphometric parameters of juvenile grass carp (*Ctenopharyngodon idellus*).[1]

Item	Dietary D-mannose level, g/kg						*P*-value
	0.52 (control)	1.75	3.02	4.28	5.50	6.78	
Growth performance							
IBW, g/fish	16.20 ± 0.010	16.19 ± 0.017	16.20 ± 0.012	16.19 ± 0.013	16.20 ± 0.016	16.20 ± 0.012	0.873
FBW, g/fish	209.50 ± 3.940	221.50 ± 3.777	226.71 ± 14.149	227.54 ± 13.100	223.01 ± 14.441	225.34 ± 13.955	0.185
PWG, %	1193.35 ± 24.868	1267.80 ± 23.474	1299.84 ± 87.280	1305.35 ± 80.904	1276.85 ± 88.156	1290.97 ± 86.312	0.182
SGR, %/d	3.66 ± 0.028	3.74 ± 0.024	3.77 ± 0.088	3.77 ± 0.081	3.74 ± 0.088	3.76 ± 0.088	0.159
FI, g/fish	287.83 ± 4.903^{a}	306.10 ± 1.153^{c}	320.73 ± 5.367^{e}	310.71 ± 2.773^{d}	302.02 ± 2.304^{c}	293.88 ± 0.329^{b}	< 0.001
FCR	1.49 ± 0.021	1.49 ± 0.030	1.53 ± 0.082	1.47 ± 0.089	1.47 ± 0.089	1.41 ± 0.091	0.255
Survival rate, %	100.00 ± 0.000	100.00 ± 0.000	100.00 ± 0.000	99.60 ± 0.894	100.00 ± 0.000	99.60 ± 0.894	0.561
Nutrient conversion rates							
PER, %	2.16 ± 0.030	2.16 ± 0.043	2.11 ± 0.120	2.19 ± 0.136	2.20 ± 0.144	2.29 ± 0.151	0.270
PRV, %	45.41 ± 0.621	48.74 ± 0.949	45.37 ± 2.503	48.29 ± 2.926	45.79 ± 2.932	46.48 ± 3.001	0.123
LPV, %	160.70 ± 2.132^{a}	186.77 ± 3.520^{c}	175.45 ± 9.275^{b}	174.30 ± 10.210^{b}	172.08 ± 10.586^{b}	173.71 ± 10.784^{b}	0.004
Whole-body nutritional components							
Moisture, %	69.30 ± 2.476	67.48 ± 2.161	67.47 ± 1.438	67.66 ± 0.486	68.59 ± 0.971	68.56 ± 1.408	0.303
CP, %	20.52 ± 1.918^{ab}	22.00 ± 1.196^{c}	21.00 ± 0.849^{abc}	21.53 ± 0.326^{bc}	20.34 ± 1.123^{ab}	19.89 ± 0.491^{a}	0.026
CL, %	10.24 ± 0.989	11.93 ± 1.177	11.48 ± 1.136	11.01 ± 0.691	10.79 ± 0.774	10.49 ± 0.975	0.052
Ash, %	2.70 ± 0.126^{a}	2.82 ± 0.122^{ab}	2.85 ± 0.167^{ab}	2.95 ± 0.071^{bc}	2.97 ± 0.139^{bc}	3.05 ± 0.156^{c}	0.001
Morphometric parameters							
HW, g/fish	7.49 ± 0.431^{a}	8.38 ± 0.214^{b}	8.73 ± 0.542^{bc}	9.17 ± 0.844^{c}	8.50 ± 0.304^{b}	8.39 ± 0.349^{b}	< 0.001
HSI, %	3.68 ± 0.114	3.75 ± 0.237	3.78 ± 0.310	3.95 ± 0.259	3.73 ± 0.283	3.46 ± 0.386	0.119
IL, cm/fish	30.15 ± 1.086^{a}	32.45 ± 1.060^{b}	32.93 ± 0.450^{b}	33.63 ± 1.147^{b}	33.30 ± 2.070^{b}	33.19 ± 1.845^{b}	0.002
IW, g/fish	6.14 ± 0.525^{a}	6.82 ± 0.529^{b}	7.22 ± 0.538^{bc}	7.72 ± 0.441^{c}	7.18 ± 0.323^{bc}	7.00 ± 0.272^{b}	< 0.001
ISI, %	2.98 ± 0.265	3.01 ± 0.258	3.19 ± 0.350	3.38 ± 0.280	3.14 ± 0.326	3.00 ± 0.289	0.180

IBW = initial body weight; FBW = final body weight; PWG = percent weight gain; SGR = specific growth rate; FI = feed intake; FCR = feed conversion ratio; PER = protein efficiency ratio; PRV = protein retention value; LPV = lipid production value; CP = crude protein; CL = crude lipid; HW = hepatosomatic weight; HSI = hepatosomatic index; IL = intestinal length; IW = intestinal weight; ISI = intestinal somatic index.
[1] Values are means ± SD (n = 6), and values within the same row with different superscripts are significantly different (P < 0.05).

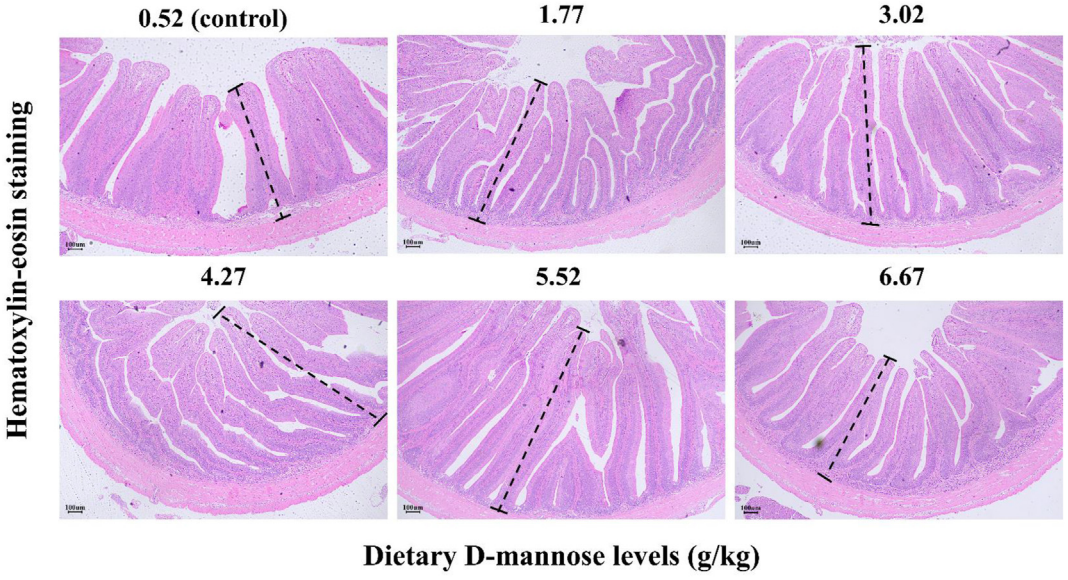

Fig. 1. Effects of D-mannose on the intestinal morphology by hematoxylin-eosin (HE) staining (40 ×, scale bars = 100 μm) of juvenile grass carp.

Table 4
Effects of D-mannose on intestinal fold height and D-mannose content as well as serum mucosal permeability indices in juvenile grass carp (*Ctenopharyngodon idellus*).[1]

Item	Dietary D-mannose level, g/kg						*P*-value
	0.52 (control)	1.75	3.02	4.28	5.50	6.78	
Fold height, μm	1115.02 ± 56.691^{a}	1200.84 ± 76.326^{ab}	1362.86 ± 149.133^{c}	1399.65 ± 137.613^{c}	1306.80 ± 130.019^{bc}	1202.19 ± 47.850^{ab}	< 0.001
D-mannose, mg/g	0.06 ± 0.004^{a}	0.07 ± 0.009^{b}	0.14 ± 0.007^{d}	0.18 ± 0.005^{f}	0.16 ± 0.020^{e}	0.11 ± 0.020^{c}	< 0.001
DAO, U/L	10.17 ± 0.261^{d}	9.90 ± 0.785^{cd}	8.77 ± 0.746^{ab}	8.27 ± 0.655^{a}	9.25 ± 0.818^{bc}	9.19 ± 0.799^{bc}	0.001
D-lactate, U/L	77.18 ± 4.465^{bc}	72.23 ± 2.518^{ab}	70.24 ± 7.335^{a}	73.06 ± 4.091^{ab}	78.24 ± 2.452^{c}	79.32 ± 0.975^{c}	0.003

DAO = diamine oxidase.
[1] Values are means ± SD (n = 6), and different superscripts in the same row are significantly different (P < 0.05).

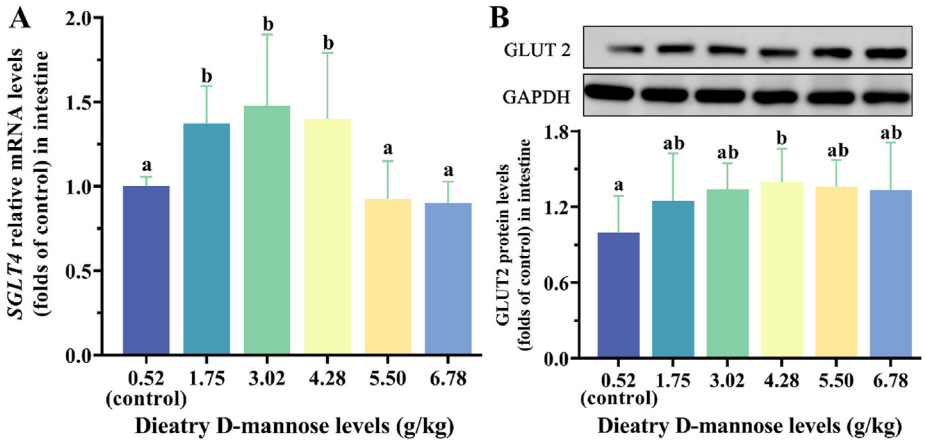

Fig. 2. Effects of D-mannose on the intestinal D-mannose-related transporters of juvenile grass carp. (A) Relative mRNA expression levels of sodium-glucose linked transporter 4 (*SGLT4*). (B) Relative protein expression levels of facilitative glucose transporter 2 (GLUT2). Data represent means of six fish in each group, error bars indicate SD. [a,b] Values with different letters are significantly different ($P < 0.05$). GAPDH = glyceraldehyde-3-phosphate dehydrogenase.

Table 5
Effects of D-mannose on intestinal glycolysis and glycosylation-related indices in juvenile grass carp (*Ctenopharyngodon idellus*).[1]

Item	Dietary D-mannose level, g/kg						*P*-value
	0.52 (control)	1.75	3.02	4.28	5.50	6.78	
PMI, ng/mg prot	5.98 ± 0.576^{b}	6.35 ± 0.608^{c}	5.46 ± 0.445^{ab}	5.11 ± 0.348^{a}	5.12 ± 0.468^{a}	5.38 ± 0.409^{a}	< 0.001
PMM, ng/mg prot	13.56 ± 1.068^{a}	16.16 ± 1.362^{b}	17.88 ± 1.228^{c}	18.19 ± 0.658^{c}	12.77 ± 1.252^{a}	13.23 ± 1.237^{a}	< 0.001
HK, U/mg prot	4.19 ± 0.271^{a}	6.51 ± 0.566^{b}	7.48 ± 0.740^{b}	13.53 ± 1.458^{d}	10.10 ± 1.235^{c}	9.57 ± 0.904^{c}	< 0.001
PFK, U/mg prot	32.14 ± 2.970^{bc}	33.46 ± 2.974^{c}	35.00 ± 1.682^{c}	29.57 ± 2.252^{ab}	26.58 ± 2.206^{a}	27.11 ± 2.195^{a}	< 0.001
PK, U/g prot	10.01 ± 1.024^{a}	16.74 ± 1.648^{c}	20.29 ± 1.889^{d}	37.70 ± 2.508^{e}	17.03 ± 2.386^{c}	14.32 ± 1.249^{b}	< 0.001
LDH, U/g prot	5.24 ± 0.484^{a}	6.09 ± 0.626^{ab}	13.22 ± 1.075^{d}	13.12 ± 0.835^{d}	11.97 ± 1.130^{c}	6.51 ± 0.539^{b}	< 0.001
LD, mmol/g prot	0.34 ± 0.030^{d}	0.30 ± 0.029^{c}	0.18 ± 0.014^{a}	0.25 ± 0.016^{b}	0.26 ± 0.018^{b}	0.30 ± 0.017^{c}	< 0.001

PMI = phosphomannose isomerase; PMM = phosphomannomutase; HK = hexokinase; PFK = phosphofructokinase; PK = pyruvate kinase; LDH = lactate dehydrogenase; LD = lactate.
[1] Values are means ± SD ($n = 6$), and different superscripts in the same row are significantly different ($P < 0.05$).

control group ($P < 0.05$) (Table 6). The intestinal T-AOC reached a maximum with D-mannose supplementation at 3.02 g/kg. With D-mannose supplementation at 4.28 g/kg, the maximum activities of CAT and GPx in fish intestines were observed. The addition of 1.75 g/kg D-mannose significantly increased the intestinal GSH content compared to the control group ($P < 0.001$).

3.4. Influence of D-mannose on the ERS-related parameter

Fig. 3A and B shows that D-mannose supplementation at 4.28 g/kg significantly reduced the mean fluorescence density of intestinal amyloid compared to the control group ($P < 0.05$). Immunofluorescence results revealed that the mean fluorescence density of intestinal GRP78 significantly decreased with increasing D-mannose levels compared to the control group ($P < 0.05$). When the D-mannose level was 3.02 g/kg, the mRNA relative levels of *GRP78*, RNA-dependent protein kinase-like ER kinase (*PERK*), eukaryotic initiation factor 2 (*EIF2A*), activating transcription factor 4 (*ATF4*), activating transcription factor 6 (*ATF6*), and inositol-requiring enzyme 1 (*IRE1*) in fish intestines were significantly reduced compared to the control group ($P < 0.05$). At the D-mannose level of 4.28 g/kg, the *CHOP* and X box-binding protein 1 (*XBP1*) mRNA relative levels in fish intestines decreased to the lowest point (Fig. 3C). The fluorescence data in Fig. 3D shows that the 4.28 g/kg addition of D-mannose significantly increased the mean fluorescence density of intestinal glycosylated proteins compared to the

Table 6
Effects of D-mannose on intestinal glycolysis-related indices in juvenile grass carp (*Ctenopharyngodon idellus*).[1]

Item	Dietary D-mannose level, g/kg						*P*-value
	0.52 (control)	1.75	3.02	4.28	5.50	6.78	
ROS, % DCF fluorescence	100.00 ± 6.600^{f}	62.86 ± 4.430^{e}	45.82 ± 3.179^{c}	24.57 ± 1.076^{a}	32.00 ± 2.161^{b}	51.12 ± 4.714^{d}	< 0.001
MDA, nmol/mg prot	4.90 ± 0.474^{b}	4.41 ± 0.409^{b}	3.83 ± 0.291^{a}	3.51 ± 0.252^{a}	4.73 ± 0.488^{b}	5.56 ± 0.435^{c}	< 0.001
PC, nmol/mg prot	1.42 ± 0.128^{c}	1.08 ± 0.127^{b}	1.03 ± 0.096^{b}	0.53 ± 0.048^{a}	0.52 ± 0.072^{a}	1.10 ± 0.070^{b}	< 0.001
T-AOC, U/mg prot	1.06 ± 0.106^{c}	1.08 ± 0.090^{c}	1.25 ± 0.094^{d}	1.07 ± 0.100^{c}	0.95 ± 0.087^{b}	0.73 ± 0.055^{a}	< 0.001
SOD, U/mg prot	13.91 ± 0.573	14.60 ± 0.959	14.50 ± 0.859	14.33 ± 0.934	14.03 ± 0.668	13.92 ± 1.496	0.706
CAT, U/mg prot	0.33 ± 0.049^{a}	0.83 ± 0.060^{c}	0.94 ± 0.091^{d}	1.48 ± 0.150^{e}	0.59 ± 0.071^{b}	0.58 ± 0.046^{b}	< 0.001
GPx, U/mg prot	53.30 ± 5.260^{a}	60.84 ± 5.634^{a}	71.06 ± 5.719^{b}	114.96 ± 7.741^{c}	58.63 ± 9.727^{a}	57.26 ± 1.624^{a}	< 0.001
GSH, mg/g prot	3.76 ± 0.162^{b}	4.50 ± 0.471^{c}	3.55 ± 0.306^{b}	3.60 ± 0.316^{b}	3.39 ± 0.221^{ab}	3.07 ± 0.223^{a}	< 0.001

ROS = reactive oxygen species; DCF = 2′,7′-dichlorofluorescein; MDA = malondialdehyde; PC = protein carbonyl; T-AOC = total antioxidant capacity; SOD = superoxide dismutase; CAT = catalase; GPx = glutathione peroxidase; GSH = glutathione.
[1] Values are means ± SD ($n = 6$), and different superscripts in the same row are significantly different ($P < 0.05$).

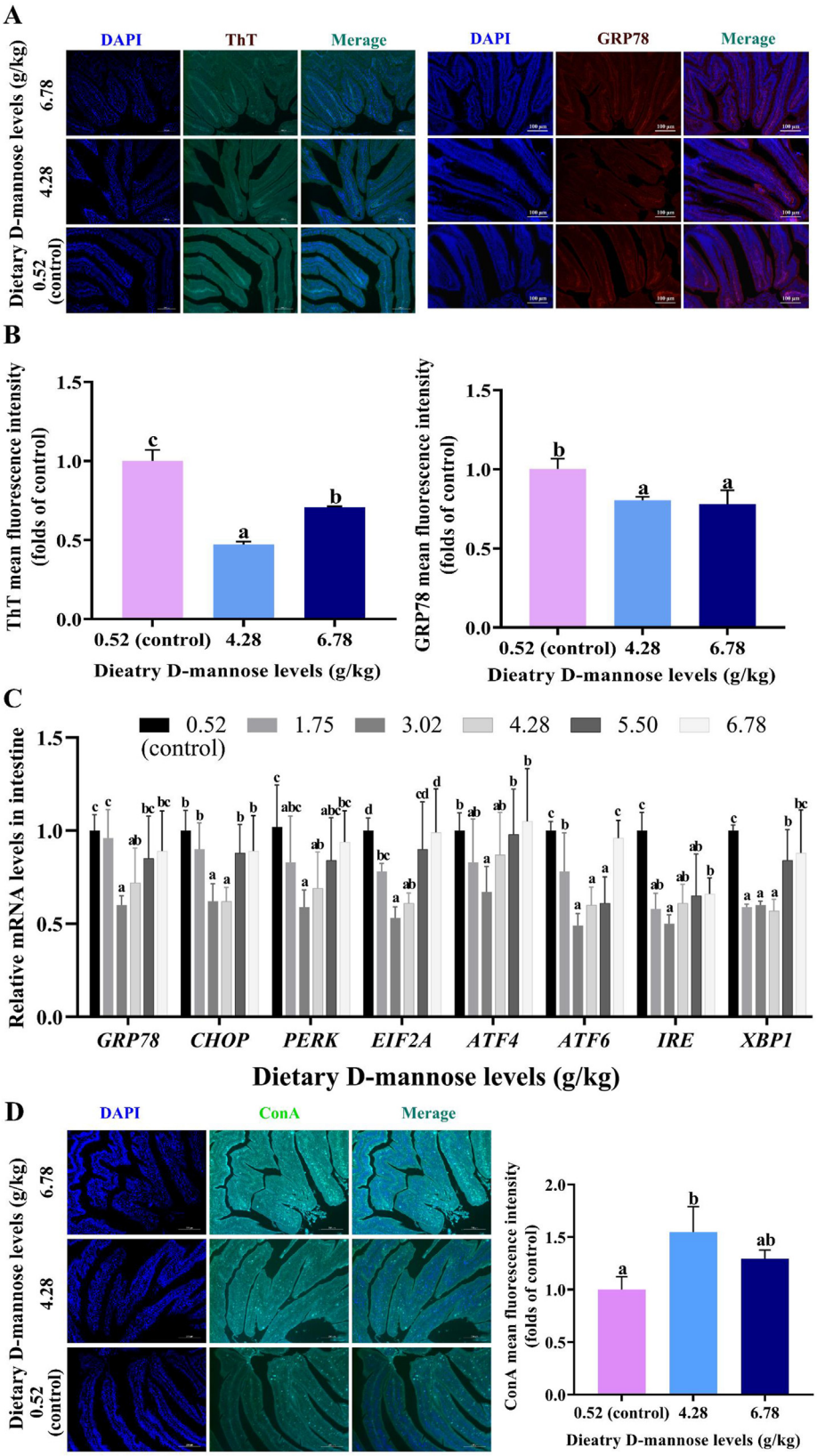

Fig. 3. Effects of D-mannose on intestinal endoplasmic reticulum stress-related indicators of juvenile grass carp. (A) Representative images of thioflavin T (ThT) stain (magnification 100 ×, scale bar = 200 μm) and glucose-regulated protein 78 (GRP78) immunofluorescence (magnification 100 ×, scale bar = 100 μm). (B) ThT and GRP78 relative fluorescence intensity statistical diagram. (C) Relative mRNA expression levels of endoplasmic reticulum stress-related proteins. (D) Representative images of concanavalin A (ConA) staining (magnification 100 ×, scale bar = 200 μm) and relative fluorescence intensity statistical diagram. Data represent means of six fish in each group, error bars indicate SD. $^{a-c}$ Values with different letters are significantly different ($P < 0.05$). DAPI = 4′,6-diamidino-2-phenylindole; CHOP=C/EBP homologous protein; PERK = protein kinase R-like endoplasmic reticulum kinase; EIF2A = eukaryotic initiation factor 2; ATF4 = activating transcription factor 4; ATF6 = activating transcription factor 6; IRE1 = inositol-requiring enzyme 1; XBP1 = X box-binding protein 1.

control group ($P < 0.05$). In Table 5, D-mannose supplementation at 4.28 g/kg significantly increased intestinal PMM activity compared to the control group ($P < 0.001$).

3.5. Influence of D-mannose on the mitophagy-related parameter

In Fig. 4A, the addition of D-mannose at 3.02 g/kg significantly increased the *PINK1* mRNA relative expression level in fish intestines compared to the control group ($P < 0.05$). The addition of D-mannose at 4.28 g/kg significantly increased the mRNA relative expression levels of BCL2 interacting protein 3-like (*BNIP3L*) and *LC3* in fish intestines compared to the control group ($P < 0.05$). With D-mannose supplementation at 4.28 g/kg, the mRNA relative expression level of *P62* in fish intestines reached a minimum.

Compared to the control group, the addition of 4.28 g/kg D-mannose significantly increased Parkin and LC3 protein levels in fish intestines ($P < 0.05$); with D-mannose supplementation at 4.28 g/kg, the protein levels of BNIP3 and FUNDC1 in fish intestines significantly increased ($P < 0.05$) (Fig. 4B).

3.6. Influence of D-mannose on AJC and AJC-linked signaling molecules

Compared to the control group, when 4.28 g/kg of D-mannose was added, the mRNA relative expression levels of *ZO-2b*, claudin-b, claudin-c, claudin-f, claudin-3c, claudin-12, junctional adhesion molecule (*JAM*), α-catenin, β-catenin, and afadin in fish intestines significantly increased ($P < 0.05$). The claudin-11 mRNA relative expression level in fish intestines reached its maximum in the 4.28 g/kg group. With the addition of D-mannose at 4.28 g/kg, the mRNA relative expression levels of claudin-15a and -15b in fish intestines were significantly reduced compared to the control group ($P < 0.05$) (Fig. 5A). As shown in Fig. 5B, the immunofluorescence results revealed that D-mannose supplementation at 4.28 g/kg significantly increased the mean fluorescence intensities of intestinal ZO-1, E-cadherin, and Nectin compared to the control group ($P < 0.05$). Meanwhile, D-mannose supplementation at 4.28 g/kg significantly increased intestinal occludin protein expression level compared to the control group ($P < 0.05$) (Fig. 5C).

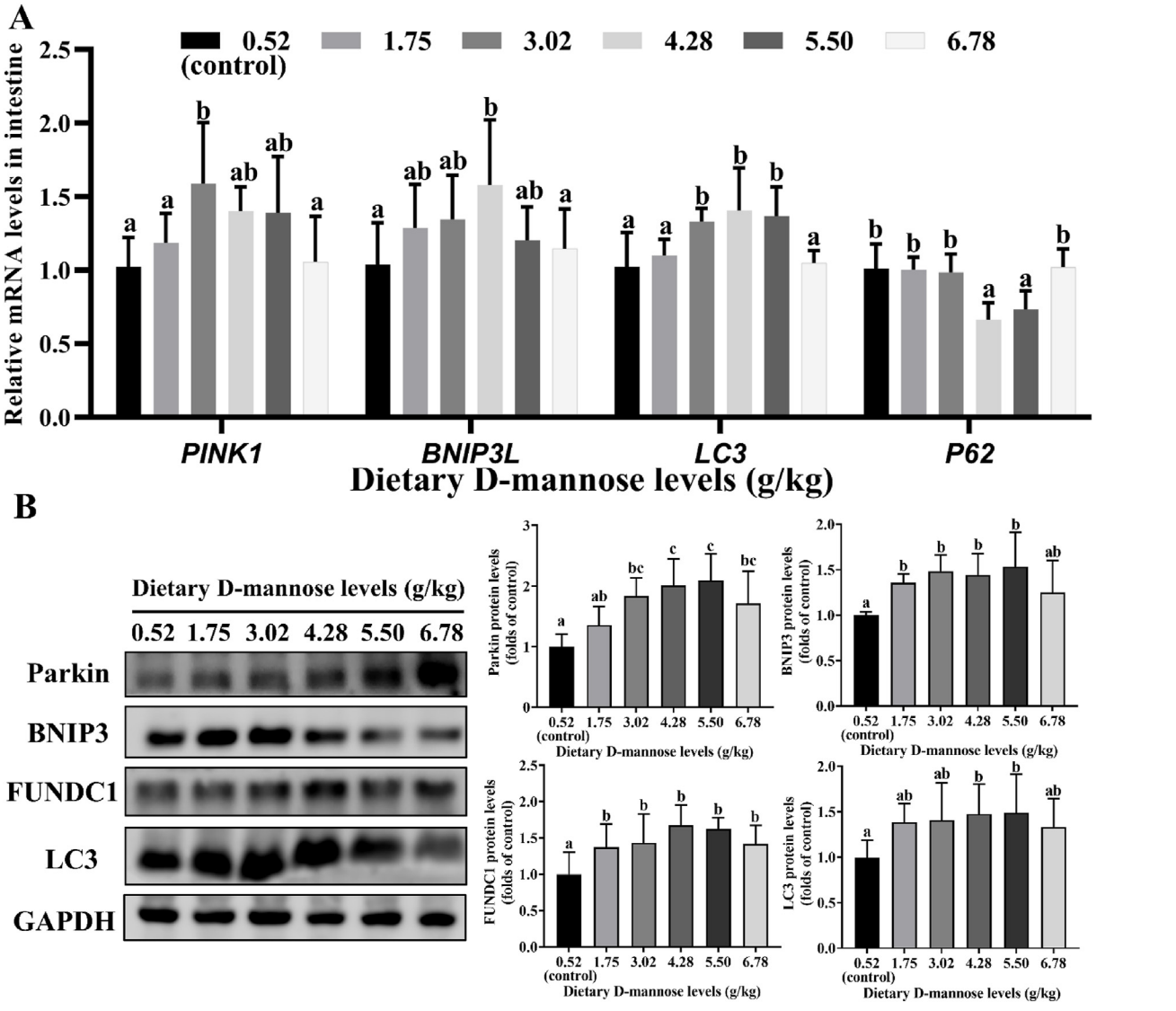

Fig. 4. Effects of D-mannose on intestinal mitophagy-related indicators of juvenile grass carp. (A) Relative mRNA expression levels of mitophagy-related proteins. (B) Relative protein expression levels. Data represent means of six fish in each group, error bars indicate SD. [a-c] Values with different letters are significantly different ($P < 0.05$). *PINK1* = PTEN-induced putative kinase 1; *BNIP3L* = BCL2 interacting protein 3-like; *LC3* = microtubule-associated protein1 light chain 3; BNIP3 = BCL2-interacting protein 3; FUNDC1 = FUN14 domain containing 1; GAPDH = glyceraldehyde-3-phosphate dehydrogenase.

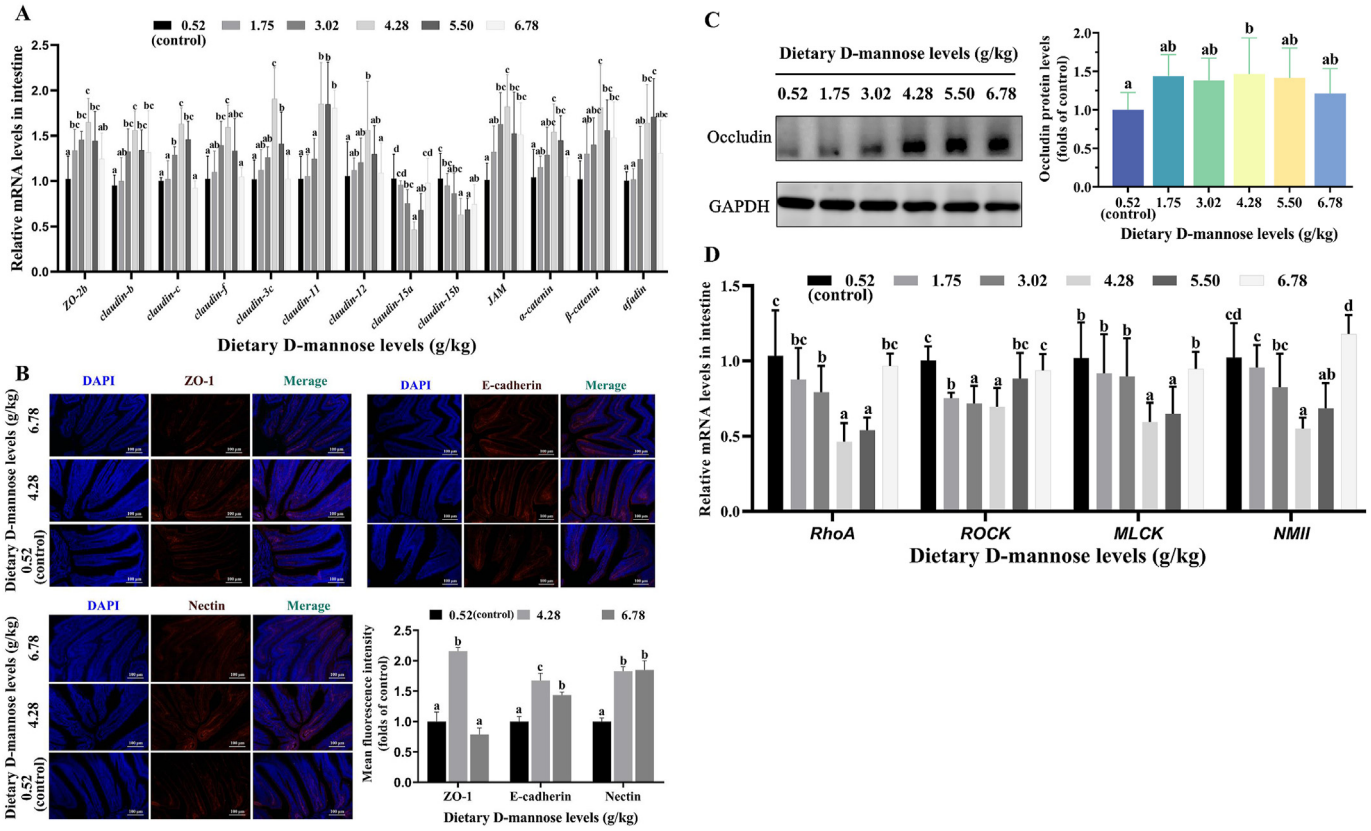

Fig. 5. Effects of D-mannose on apical junctional complex (AJC) and AJC-related signaling molecules in the intestine of juvenile grass carp. (A) Relative mRNA expression levels of AJC. (B) Zonula occludens-1 (ZO-1), E-cadherin and Nectin immunofluorescence (magnification 100 ×, scale bar = 100 μm) and relative fluorescence intensity statistical diagram. (C) Occludin relative protein expression levels. (D) Relative mRNA expression levels of AJC-related signaling molecules. Data represent means of six fish in each group, error bars indicate SD. [a-d] Values with different letters are significantly different ($P < 0.05$). ZO = zonula occludens; JAM = junctional adhesion molecule; *RhoA* = a small Rho GTPase protein; *ROCK* = Rho-associated protein kinase; *MLCK* = myosin light chain kinase; *NMII* = non-muscle myosin II.

The addition of 4.28 g/kg D-mannose significantly reduced the mRNA relative expression levels of *RhoA*, *ROCK*, *MLCK*, and non-muscle myosin II (*NMII*) in fish intestines compared to the control group ($P < 0.05$) (Fig. 5D).

4. Discussion

4.1. Dietary D-mannose enhanced growth performance and intestinal morphology in fish

Our research revealed that dietary D-mannose levels increased FI but did not affect PWG, SGR, and FCR. However, the study on zebrafish showed that feeding D-mannose for 2 weeks improved health, FI, and FCR but decreased PWG (Wang et al., 2021a). Possible reasons for this discrepancy could be variations in fish or short- and long-term feeding effects, but further research is necessary. Fish growth depends on nutrient storage (Le Mézo et al., 2022). We found that the addition of D-mannose at 1.75 or 1.75 to 6.78 g/kg increased crude protein or the lipid production value, indicating that D-mannose enhanced nutrient storage in grass carp.

Also, the growth of fish is strongly linked to the development of the gut (P Li et al., 2022). Our study found that dietary D-mannose levels at 3.02 to 5.50 g/kg increased hepatopancreas weight, intestinal length, intestinal weight, and intestinal fold height, demonstrating that D-mannose improved fish intestinal growth. The growth and development of the intestines may be attributed to the metabolism of D-mannose. In mammals, over 95% of intracellular D-mannose enters the glycolytic pathway via PMI to support biosynthetic processes (Sharma et al., 2014). The study found that dietary D-mannose levels at 3.02 to 6.78 g/kg increased intestinal HK, PK, and LDH activities, while reducing intestinal LD levels. Adding 1.75 or 1.75 to 6.78 g/kg of D-mannose raised the levels of PMI or D-mannose content in fish intestines, demonstrating that D-mannose participated in intestinal glycolysis. It has been reported that SGLT4 plays a role in the absorption of D-mannose in the intestine (Tazawa et al., 2005). Meanwhile, GLUT2 is distributed in the intestinal basolateral membrane and primarily transports monosaccharides into the bloodstream (Liang et al., 2020). We found that adding 4.28 g/kg of D-mannose increased the relative expression of *SGLT4* mRNA and GLUT2 protein in the gut, suggesting that D-mannose promoted its intestinal transit. The growth of fish intestines can only be achieved with structural integrity. Consequently, we explored the link between D-mannose and the structure of grass carp intestines.

4.2. Dietary D-mannose improved intestinal structural integrity in fish

The permeability of the intestinal mucosa can reflect its structural integrity, which is correlated with serum D-lactate content and DAO activity (Massier et al., 2021). Adding 3.02 to 6.78 or 3.02 g/kg of D-mannose reduced DAO activity or D-lactate content in the serum, indicating that D-mannose enhanced the structural integrity of the intestines. Intestinal structure can be mainly categorized into cellular structures and intercellular AJC (Yu and Li, 2014). So, we investigated the relationship between D-mannose

and the structure of fish intestinal cells, as well as the associated mechanisms.

4.3. Dietary D-mannose improved the cellular structure of the fish intestine

The destruction of cellular structures is usually associated with the accumulation of large amounts of ROS, which disrupts redox homeostasis (Augustin, 2010). Antioxidant enzymes are essential for maintaining redox homeostasis and scavenging PC and MDA (Jiang et al., 2019). We found that the optimal levels of D-mannose (3.02–4.28 g/kg) decreased intestinal ROS, PC, and MDA contents. The addition of 1.75 g/kg increased the content of GSH in fish intestines compared to the control group. Dietary D-mannose levels at 3.02 or 3.02 to 4.28 g/kg also enhanced the T-AOC or activities of CAT and GPx in the intestine of grass carp, indicating that D-mannose maintained redox homeostasis in the gut.

An imbalance in redox homeostasis is closely associated with ER stress (Görlach et al., 2006). And ThT can stain the amyloid and reflect the ER stress of the tissue (Chi et al., 2022). We demonstrated that the addition of 4.28 g/kg D-mannose reduced intestinal amyloid levels, suggesting that D-mannose alleviated ER stress in the intestine. Endoplasmic reticulum stress activates CHOP proteins through the UPR (Chen et al., 2023), and the overexpression of *CHOP* leads to oxidative damage and apoptosis (So, 2018). We found that dietary D-mannose levels at 3.02 to 4.28 g/kg reduced the mRNA relative expression level of *CHOP* in fish intestines. The transcriptional activation of CHOP is regulated by XBP1, ATF4, and ATF6 (Li et al., 2014). Adding 3.02 g/kg of D-mannose reduced the mRNA relative expression levels of *XBP1*, *ATF4*, and *ATF6* in the intestines compared to the control group. Furthermore, the mRNA relative expression level of *CHOP* was positively correlated with *XBP1*, *ATF4*, and *ATF6* (Fig. 6), suggesting that the decrease in CHOP transcription by D-mannose may be linked to the downregulation of *XBP1*, *ATF4*, and *ATF6* mRNA relative expression. Furthermore, XBP1 and ATF4 are regulated by the IRE1 and PERK-EIF2α pathways, respectively (Burton et al., 2017). We demonstrated that the addition of D-mannose at 3.02 to 4.28 g/kg reduced the mRNA relative expression levels of *IRE1*, *PERK*, and *EIF2α* in fish intestines. The transcription level of *XBP1* was positively correlated with *IRE1*, while the mRNA relative expression level of *ATF4* was positively correlated with *EIF2A* and *PERK* (Fig. 6), suggesting that the decrease in *XBP1* and *ATF4* mRNA relative expression levels by D-mannose may be associated with the inhibition of the IRE1 and PERK-EIF2A pathways. It has been reported that XBP1, ATF4, and ATF6 are activated by the GRP78 chaperone when dissociated from the UPR-related protein complexes (Burton et al., 2017). The addition of 4.28 g/kg D-mannose decreased the mRNA relative expression level and fluorescence intensity of GRP78 in fish intestines. Our study demonstrated that D-mannose inhibited the UPR pathway of ER stress in the intestine of juvenile grass carp. We suggested that D-mannose repressed the UPR pathway of ER stress, possibly related to protein glycosylation. Protein glycosylation processes are essential for controlling protein quantity (Roth et al., 2010). We found that the addition of 4.28 g/kg D-mannose increased the levels of intestinal protein glycosylation recognized by ConA staining in juvenile grass carp, confirming our previous hypothesis. Further, we suggested that D-mannose increased protein glycosylation, possibly in close association with PMM. In mammalian cells, PMM is an essential enzyme in protein glycosylation (Sharma et al., 2014). Our research showed that dietary D-mannose levels at 1.75 to 4.28 g/kg improved the PMM level in the gut. Correlation analysis revealed a strong correlation between protein glycosylation and the PMM level, suggesting that enhanced protein glycosylation may be related to PMM. We concluded that D-mannose inhibited the UPR pathway of ER stress, including the IRE1, PERK, and ATF6 pathways, which may be associated with enhanced protein glycosylation. Furthermore, mitophagy is essential for maintaining cellular redox homeostasis (Garza-Lombó et al., 2020). Next, the study investigated the impact of D-mannose on mitophagy.

Mitophagy is a cellular self-protection mechanism that involves removing damaged mitochondria (Saita et al., 2013). The damaged mitochondria are phagocytosed by vesicles encapsulated by the autophagosome marker LC3 (Cao et al., 2020). Furthermore, P62 is primarily responsible for degrading ubiquitinated mitochondria (Geisler et al., 2010). Adding 4.28 to 5.50 g/kg of D-mannose increased the mRNA and protein relative expression levels of LC3 and decreased the mRNA relative expression level of *P62* in fish intestines, demonstrating that D-mannose could enhance mitophagy. The mechanisms of mitophagy can be categorized into Ub-dependent and Ub-independent pathways (Wang et al., 2021b). The Ub-dependent mitophagy primarily relies on the PINK1/Parkin pathway (A Li et al., 2022).

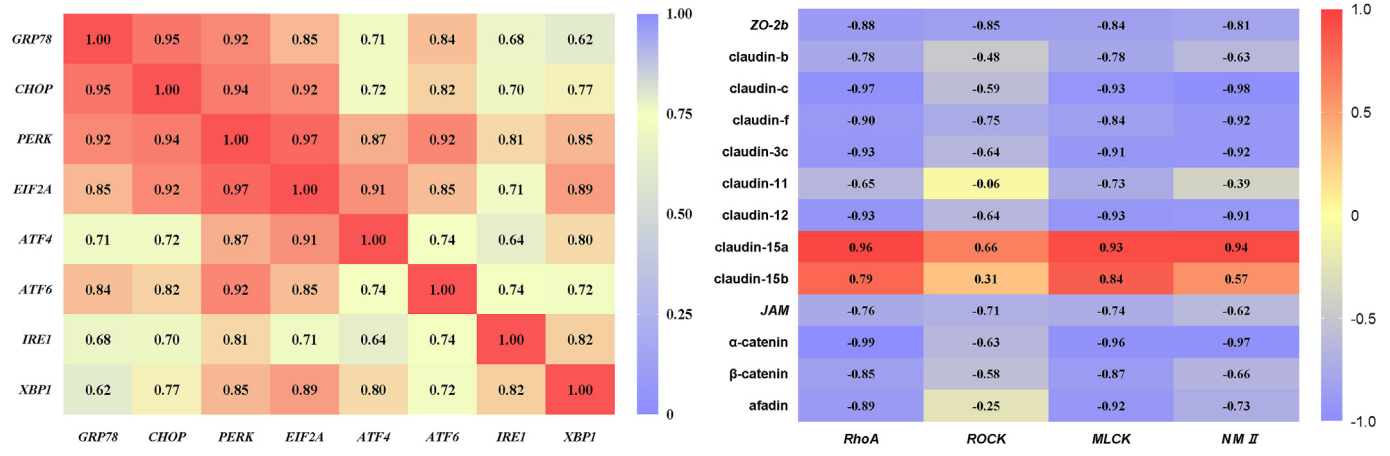

Fig. 6. The parameters of correlation analysis of endoplasmic reticulum stress-related and apical junctional complex-related gene expression in the intestine of grass carp. The numbers represent Pearson values. GRP78 = glucose regulatory protein 78; CHOP = C/EBP homologous protein; PERK = protein kinase R-like endoplasmic reticulum kinase; EIF2A = eukaryotic initiation factor 2; ATF4 = activating transcription factor 4; ATF6 = activating transcription factor 6; IRE1 = inositol-requiring enzyme 1; XBP1 = X box-binding protein-1; ZO = zonula occludens; JAM = junctional adhesion molecule; RhoA = a small Rho GTPase protein; ROCK = Rho-associated protein kinase; MLCK = myosin light chain kinase; NMII = non-muscle myosin II.

We demonstrated that dietary D-mannose levels at 3.02 or 3.02 to 6.78 g/kg increased *PINK1* mRNA relative expression level or Parkin protein level in fish intestines. The Ub-dependent mitophagy is primarily mediated directly by three receptors, including the BNIP3L receptor, BNIP3 receptor, and FUNDC1 receptor (Lu et al., 2023). Adding 4.28 g/kg of D-mannose increased the expression levels of *BNIP3L* mRNA, BNIP3, and FUNDC1 protein in fish intestines. The results above suggested that D-mannose promoted mitophagy through Ub-dependent pathways (PINK1/Parkin) and Ub-independent pathways (BNIP3L, BNIP3, and FUNDC1). The structural integrity of the gut is closely related to the intestinal AJC. Therefore, we set out to investigate the effects and possible mechanisms of D-mannose on the AJC of fish.

4.4. Dietary D-mannose improved the AJC of the fish intestine probably mediated by RhoA/ROCK signaling

Tight junction can be categorized into barrier-forming and pore-forming TJ, which are essential for maintaining intestinal structure (Dai et al., 2023). Our findings showed that adding 4.28 g/kg of D-mannose increased the expression levels of intestinal ZO-1 and occludin proteins in fish. We also demonstrated that adding 4.28 g/kg of D-mannose increased the mRNA relative expression levels of barrier-forming TJ (*ZO-2b*, claudin-b, claudin-c, claudin-f, claudin-3c, claudin-11, and *JAM*) in fish intestines. In contrast, D-mannose supplementation reduced the mRNA relative expression levels of the pore-forming TJ (claudin-15a and claudin-15b) in fish intestines. The above results indicated that D-mannose could enhance the intestinal TJ structure of fish.

Curiously, our study identified a differentially expressed gene. Claudin-12 is recognized as a TJ protein involved in pore formation, and the decrease in claudin-12 levels may be linked to the reinforcement of the TJ structure (Zhang et al., 2023). In our study, the mRNA relative expression level of claudin-12 in fish intestines was enhanced by adding 4.28 g/kg of D-mannose. The likely cause of this discrepancy is related to Ca^{2+} homeostasis. Claudin-12 has been reported to be critical in intestinal Ca^{2+} transport (Beggs et al., 2021). Ca^{2+} homeostasis is closely related to ER function (Krebs et al., 2015). This suggests that the increase in claudin-12 induced by D-mannose may be more related to the regulation of calcium balance to reduce ER stress. However, more in-depth studies are required.

In addition, the formation of AJ depends on the action of cadherin and Nectin (Campbell et al., 2017). Immunofluorescence analysis revealed that adding 4.28 g/kg of D-mannose increased the expression levels of E-cadherin and Nectin proteins in the fish intestine. In our study, dietary D-mannose levels at 4.28 to 5.50 g/kg also increased the mRNA relative expression levels of α-catenin, β-catenin, and afadin in the intestine. These results showed that D-mannose improved the intestinal AJ structure of fish.

The TJ and AJ together form the AJC, which functions to maintain intercellular structure (González-Mariscal et al., 2020). Our study revealed, for the first time, that D-mannose may strengthen TJ and AJ structures, thereby enhancing intestinal AJC structure. The integrity of the AJC structure is regulated by the MLCK-mediated contraction of actomyosin (Du et al., 2016). For the first time, our research observed that dietary D-mannose levels at 4.28 g/kg reduced the mRNA relative expression levels of *RhoA*, *ROCK*, *MLCK*, and *NMII* in fish intestines. Further correlation analysis revealed a negative correlation between the mRNA relative expression levels of barrier-forming AJC and RhoA/ROCK-related signaling molecules. In contrast, a positive correlation was found between the mRNA relative expression levels of pore-forming TJ (except claudin-12) and RhoA/ROCK-related signaling molecules (Fig. 6). Overall, these results indicated that D-mannose improved the TJ and AJ structures of the AJC, partly due to the inhibition of RhoA/ROCK signaling.

4.5. Optimum addition of D-mannose in fish

The optimal level of additives for growth performance is essential for grass carp culture and formulation (Lu et al., 2020). Based on the regression analysis of the PWG ($y = -6.164x^2 + 56.82x + 1175$, $R^2 = 0.8686$, $P < 0.05$), the optimal addition of D-mannose was 4.61 g/kg for juvenile grass carp (Fig. S1). In line with our findings, the only study in fish showed that the optimal addition of D-mannose for zebrafish health was 5 g/kg (Wang et al., 2021a). It has been reported that ROS is a marker of redox homeostasis and is essential for determining the nutritional requirements for fish disease resistance (Jiang et al., 2017). The regression analysis of intestinal ROS content ($y = 4.325x^2 - 39.7x + 120.2$, $R^2 = 0.9819$, $P < 0.01$) suggested that the optimal addition of D-mannose to juvenile grass carp was 4.59 g/kg (Fig. S1). The above results indicated that the optimal addition of D-mannose, as determined by oxidative damage and growth performance, was similar. This may be because growth performance is closely linked to gut health, and improved gut health promotes better growth. A similar result was found for the optimal addition of arecoline, as determined based on PWG and oxidative damage indicators by Yao et al. (2023).

5. Conclusions

In conclusion, our study showed that D-mannose improved fish growth performance and body composition. At the same time, we found that D-mannose improved the intestinal growth and development of fish, which may be related to the enhancement of glycolysis by PMI. To the best of our knowledge, this is the first time that D-mannose has been found to improve the cellular and intercellular structure of the intestine. The enhancement of cellular redox homeostasis involves alleviating the UPR pathway of ER stress, possibly associated with the PMM-mediated enhancement of glycosylation levels. Ub-dependent and Ub-independent mitophagy may also play a role. The improvement of the intercellular structure involves improving the TJ and AJ structures of the AJC, which may be closely related to the RhoA/ROCK pathway. Finally, regression analysis of the PWG and intestinal ROS content suggested that the optimal addition of D-mannose to juvenile grass carp was 4.61 and 4.59 g/kg, respectively.

Author contributions

Chong Zhang: Manuscript writing, Formal analysis; **Lin Feng:** Conceptualization, Funding Acquisition, Supervision; **Pei Wu:** Conceptualization, Methodology, Validation, Data Curation and Project Administration; **Yang Liu:** Methodology; **Xiaowan Jin and Hongmei Ren:** Management; **Hua Li and Fali Wu:** Research Design and Coordination; **Xiaoqiu Zhou:** Conceptualization, Methodology, Supervision, Funding Acquisition and Resources; **Weidan Jiang:** Data Curation, Validation, Supervision, Project Administration and Writing - review & editing. Xiaoqiu Zhou and Weidan Jiang had primary responsibility for the final content of the manuscript. All authors carefully read and approved the final revision of the manuscript.

Declaration of competing interest

We declare that we have no financial and personal relationships with other people or organizations that might inappropriately influence our work, and there is no professional or other personal

interest of any nature or kind in any product, service and/or company that could be construed as influencing the content of this paper.

Acknowledgements

This research was financially supported by the earmarked fund for CARS (CARS-45), and the National Key R&D Program of China (2019YFD0900200). The authors would like to thank the personnel of these teams for their kind assistance.

Appendix Supplementary data

Supplementary data to this article can be found online at https://doi.org/10.1016/j.aninu.2024.05.003.

References

Adil MS, Narayanan SP, Somanath PR. Cell-cell junctions: structure and regulation in physiology and pathology. Tissue Barriers 2021;9(1):1848212.
Al-Sadi R, Ye D, Said HM, Ma TY. IL-1β-induced increase in intestinal epithelial tight junction permeability is mediated by MEKK-1 activation of canonical NF-kB pathway. Am J Pathol 2010;177(5):2310–22.
Aly SM, Elatta MA, ElBanna NI, El-Shiekh MA, Kelany MS, Fathi M, Mabrok M. Studies on *Vibrio campbellii* as a newly emerging pathogen affecting cultured seabream (*Sparus aurata*) in Egypt. Aquacult Int 2024;32:1685–701.
AOAC. Official methods of analysis. 18th ed. Gaithersburg, MD, USA: AOAC International; 2005.
Augustin AJ. Oxidative tissue damage. Klin Monbl Augenheilkd 2010;227(2):90–8.
Babaei-Abraki S, Karamali F, Nasr-Esfahani MH. The role of endoplasmic reticulum and mitochondria in maintaining redox status and glycolytic metabolism in pluripotent stem cells. Stem Cell Rev Rep 2022;18(5):1789–808.
Beggs MR, Young K, Pan W, O'Neill DD, Saurette M, Plain A, et al. Claudin-2 and claudin-12 form independent, complementary pores required to maintain calcium homeostasis. Proc Natl Acad Sci U S A 2021;118(48):e2111247118.
Burton GJ, Yung HW, Murray AJ. Mitochondrial-endoplasmic reticulum interactions in the trophoblast: stress and senescence. Placenta 2017;52:146–55.
Campbell HK, Maiers JL, DeMali KA. Interplay between tight junctions & adherens junctions. Exp Cell Res 2017;358(1):39–44.
Cao S, Wang C, Yan J, Li X, Wen J, Hu C. Curcumin ameliorates oxidative stress-induced intestinal barrier injury and mitochondrial damage by promoting Parkin dependent mitophagy through AMPK-TFEB signal pathway. Free Radic Biol Med 2020;147:8–22.
Cao S, Xiao H, Li X, Zhu J, Gao J, Wang L, Hu C. AMPK-PINK1/Parkin mediated mitophagy is necessary for alleviating oxidative stress-induced intestinal epithelial barrier damage and mitochondrial energy metabolism dysfunction in IPEC-J2. Antioxidants 2021;10(12):2010.
Chen X, Shi C, He M, Xiong S, Xia X. Endoplasmic reticulum stress: molecular mechanism and therapeutic targets. Signal Transduct Targeted Ther 2023;8(1):352.
Chi YN, Ye RJ, Yang JM, Hai DM, Liu N, Ren JW, et al. Geniposide attenuates spermatogenic dysfunction via inhibiting endoplasmic reticulum stress in male mice. Chem Biol Interact 2022;366:110144.
Dai QQ, Zhou XQ, Jiang WD, Wu P, Liu Y, Shi HQ, et al. Application of enzymatically treated *Artemisia annua* L. on adult grass carp (*Ctenopharyngodon idella*): improved growth performance, intestinal antioxidant capacity and apical junctional complex. Aquaculture 2023;575:739612.
Deng YP, Jiang WD, Liu Y, Jiang J, Kuang SY, Tang L, et al. Differential growth performance, intestinal antioxidant status and relative expression of Nrf2 and its target genes in young grass carp (*Ctenopharyngodon idella*) fed with graded levels of leucine. Aquaculture 2014;434:66–73.
Dong L, Xie J, Wang Y, Jiang H, Chen K, Li D, et al. Mannose ameliorates experimental colitis by protecting intestinal barrier integrity. Nat Commun 2022;13(1):4804.
Du L, Kim JJ, Shen J, Dai N. Crosstalk between inflammation and ROCK/MLCK signaling pathways in gastrointestinal disorders with intestinal hyperpermeability. Gastroenterol Res Pract 2016;2016:7374197.
FAO. The state of world fisheries and aquaculture 2022. Rome: Food and Agriculture Organization of the United Nations; 2022.
Garza-Lombó C, Pappa A, Panayiotidis MI, Franco R. Redox homeostasis, oxidative stress and mitophagy. Mitochondrion 2020;51:105–17.
Geisler S, Holmström KM, Skujat D, Fiesel FC, Rothfuss OC, Kahle PJ, Springer W. PINK1/Parkin-mediated mitophagy is dependent on VDAC1 and p62/SQSTM1. Nat Cell Biol 2010;12(2):119–31.
González-Mariscal L, Miranda J, Gallego-Gutiérrez H, Cano-Cortina M, Amaya E. Relationship between apical junction proteins, gene expression and cancer. Biochim Biophys Acta Biomembr 2020;1862(9):183278.
Görlach A, Klappa P, Kietzmann DT. The endoplasmic reticulum: folding, calcium homeostasis, signaling, and redox control. Antioxidants Redox Signal 2006;8(9–10):1391–418.
Hetz C. The unfolded protein response: controlling cell fate decisions under ER stress and beyond. Nat Rev Mol Cell Biol 2012;13(2):89–102.
Homolak J, Babic Perhoc A, Knezovic A, Osmanovic Barilar J, Virag D, Joja M, Salkovic-Petrisic M. The effect of acute oral galactose administration on the redox system of the rat small intestine. Antioxidants 2021;11(1):37.
Ichikawa M, Scott DA, Losfeld ME, Freeze HH. The metabolic origins of mannose in glycoproteins. J Biol Chem 2014;289(10):6751–61.
Im K, Mareninov S, Diaz MFP, Yong WH. An introduction to performing immunofluorescence staining. Methods Mol Biol 2019;1897:299–311.
Jiang WD, Tang RJ, Liu Y, Wu P, Kuang SY, Jiang J, et al. Impairment of gill structural integrity by manganese deficiency or excess related to induction of oxidative damage, apoptosis and dysfunction of the physical barrier as regulated by NF-κB, caspase and Nrf2 signaling in fish. Fish Shellfish Immunol 2017;70:280–92.
Jiang WD, Zhou XQ, Zhang L, Liu Y, Wu P, Jiang J, et al. Vitamin A deficiency impairs intestinal physical barrier function of fish. Fish Shellfish Immunol 2019;87:546–58.
Jin Y, Blikslager AT. The regulation of intestinal mucosal barrier by myosin light chain kinase/Rho kinases. Int J Mol Sci 2020;21(10):3550.
Krebs J, Agellon LB, Michalak M. Ca^{2+} homeostasis and endoplasmic reticulum (ER) stress: an integrated view of calcium signaling. Biochem Biophys Res Commun 2015;460(1):114–21.
Kuang SY, Xiao WW, Feng L, Liu Y, Jiang J, Jiang WD, et al. Effects of graded levels of dietary methionine hydroxy analogue on immune response and antioxidant status of immune organs in juvenile Jian carp (*Cyprinus carpio* var. Jian). Fish Shellfish Immunol 2012;32(5):629–36.
Kushwaha V, Rai P, Varshney S, Gupta S, Khandelwal N, Kumar D, Gaikwad A. Sodium butyrate reduces endoplasmic reticulum stress by modulating CHOP and empowers favorable anti-inflammatory adipose tissue immune-metabolism in HFD fed mice model of obesity. Food Chem 2022;4:100079.
LeBel CP, Ischiropoulos H, Bondy SC. Evaluation of the probe 2',7'-dichlorofluorescein as an indicator of reactive oxygen species formation and oxidative stress. Chem Res Toxicol 1992;5:227–31.
Le Mézo P, Guiet J, Scherrer K, Bianchi D, Galbraith E. Global nutrient cycling by commercially targeted marine fish. Biogeosciences 2022;19(10):2537–55.
Li A, Gao M, Liu B, Qin Y, chen L, Liu H, et al. Mitochondrial autophagy: molecular mechanisms and implications for cardiovascular disease. Cell Death Dis 2022;13(5):444.
Li P, Hou D, Zhao H, Wang H, Peng K, Cao J. Dietary *Clostridium butyricum* improves growth performance and resistance to ammonia stress in yellow catfish (*Pelteobagrus fulvidraco*). Aquacult Nutr 2022;2022:6965174.
Li Y, Guo Y, Tang J, Jiang J, Chen Z. New insights into the roles of CHOP-induced apoptosis in ER stress. Acta Biochim Biophys Sin 2014;46(8):629–40.
Liang X, Yan F, Gao Y, Xiong M, Wang H, Onxayvieng K, et al. Sugar transporter genes in grass carp (*Ctenopharyngodon idellus*): molecular cloning, characterization, and expression in response to different stocking densities. Fish Physiol Biochem 2020;46(3):1039–52.
Lin Z, Miao J, Zhang T, He M, Zhou X, Zhang H, et al. D-Mannose suppresses osteoarthritis development in vivo and delays IL- 1β-induced degeneration in vitro by enhancing autophagy activated via the AMPK pathway. Biomed Pharmacother 2021;135:111199.
Livak KJ, Schmittgen TD. Analysis of relative gene expression data using real-time quantitative PCR and the $2^{-\Delta\Delta CT}$ Method. Methods 2001;25(4):402–8.
Loke I, Kolarich D, Packer NH, Thaysen-Andersen M. Emerging roles of protein mannosylation in inflammation and infection. Mol Aspect Med 2016;51:31–55.
Lu Y, Li Z, Zhang S, Zhang T, Liu Y, Zhang L. Cellular mitophagy: mechanism, roles in diseases and small molecule pharmacological regulation. Theranostics 2023;13(2):736–66.
Lu ZY, Feng L, Jiang WD, Wu P, Liu Y, Kuang SY, et al. Mannan oligosaccharides improved growth performance and antioxidant capacity in the intestine of on-growing grass carp (*Ctenopharyngodon idella*). Aquac Rep 2020;17:100313.
Ma R, Feng L, Wu P, Liu Y, Ren HM, Li SW, et al. A new insight on copper: promotion of collagen synthesis and myofiber growth and development in juvenile grass carp (*Ctenopharyngodon idella*). Anim Nutr 2023;15:22–33.
Massier L, Blüher M, Kovacs P, Chakaroun RM. Impaired intestinal barrier and tissue bacteria: pathomechanisms for metabolic Diseases. Front Endocrinol 2021;12.
NRC (National Research Council). Nutrient requirements of fish and shrimp. Washington (DC): The National Academy Press; 2011.
Palikaras K, Lionaki E, Tavernarakis N. Mechanisms of mitophagy in cellular homeostasis, physiology and pathology. Nat Cell Biol 2018;20(9):1013–22.
Pang A, Xin Y, Xie R, Wang Z, Zhang W, Tan B. Differential analysis of fish meal substitution with two soybean meals on juvenile pearl gentian grouper. Front Mar Sci 2023;10:1170033.
Qin Y, Zhong Y, Yang G, Ma T, Jia L, Huang C, Li Z. Profiling of concanavalin A-binding glycoproteins in human hepatic stellate cells activated with transforming growth factor-β1. Molecules 2014;19(12):19845–67.
Roth J. Lectins for histochemical demonstration of glycans. Histochem Cell Biol 2011;136(2):117–30.
Roth J, Zuber C, Park S, Jang I, Lee Y, Kysela KG, et al. Protein N-glycosylation, protein folding, and protein quality control. Mol Cell 2010;30(6):497–506.
Saita S, Shirane M, Nakayama KI. Selective escape of proteins from the mitochondria during mitophagy. Nat Commun 2013;4(1):1410.

Scaglione F, Musazzi UM, Minghetti P. Considerations on D-mannose mechanism of action and consequent classification of marketed healthcare products. Front Pharmacol 2021;12:636377.
Sharma V, Ichikawa M, Freeze HH. Mannose metabolism: more than meets the eye. Biochem Biophys Res Commun 2014;453(2):220–8.
So JS. Roles of endoplasmic reticulum stress in immune responses. Mol Cell 2018;41(8):705–16.
Soyama K. Enzymatic determination of D-mannose in serum. Clin Chem 1984;302:293–4.
Tazawa S, Yamato T, Fujikura H, Hiratochi M, Itoh F, Tomae M, et al. SLC5A9/SGLT4, a new Na^+-dependent glucose transporter, is an essential transporter for mannose, 1,5-anhydro-D-glucitol, and fructose. Life Sci 2005;76(9):1039–50.
Tie HM, Wu P, Jiang WD, Liu Y, Kuang SY, Zeng YY, et al. Dietary nucleotides supplementation affect the physicochemical properties, amino acid and fatty acid constituents, apoptosis and antioxidant mechanisms in grass carp (*Ctenopharyngodon idellus*) muscle. Aquaculture 2019;502:312–25.
Torretta S, Scagliola A, Ricci L, Mainini F, Di Marco S, Cuccovillo I, et al. D-mannose suppresses macrophage IL-1β production. Nat Commun 2020;11(1):6343.
Vial E, Sahai E, Marshall CJ. ERK-MAPK signaling coordinately regulates activity of Rac1 and RhoA for tumor cell motility. Cancer Cell 2003;4(1):67–79.
Wang A, Zhang Z, Ding Q, Yang Y, Bindelle J, Ran C, Zhou Z. Intestinal *Cetobacterium* and acetate modify glucose homeostasis via parasympathetic activation in zebrafish. Gut Microb 2021a;13(1):1–15.
Wang H, Zheng Y, Huang J, Li J. Mitophagy in antiviral immunity. Front Cell Dev Biol 2021b;9:723108.
Wang J, Jalali Motlagh N, Wang C, Wojtkiewicz GR, Schmidt S, Chau C, et al. D-mannose suppresses oxidative response and blocks phagocytosis in experimental neuroinflammation. Proc Natl Acad Sci U S A 2021c;118(44):e2107663118.
Wang ST, Meng XZ, Li LS, Dang YF, Fang Y, Shen Y, et al. Biological parameters, immune enzymes, and histological alterations in the livers of grass carp infected with *Aeromonas hydrophila*. Fish Shellfish Immunol 2017;70:121–8.
Wang Y, Xie S, He B. Mannose shows antitumour properties against lung cancer via inhibiting proliferation, promoting cisplatin-mediated apoptosis and reducing metastasis. Mol Med Rep 2020;22(4):2957–65.
Wei Z, Huang L, Cui L, Zhu X. Mannose: good player and assister in pharmacotherapy. Biomed Pharmacother 2020;129:110420.
Xiao P, Hu Z, Lang J, Pan T, Mertens RT, Zhang H, et al. Mannose metabolism normalizes gut homeostasis by blocking the TNF-α-mediated proinflammatory circuit. Cell Mol Immunol 2022;20(2):119–30.
Xue X, Zhou XQ, Wu P, Jiang WD, Liu Y, Zhang RN, Feng L. New perspective into possible mechanism in growth promotion of potassium diformate (KDF) on the juvenile grass carp (*Ctenopharyngodon idella*). Aquaculture 2023;576:739850.
Yao K, Feng L, Jiang WD, Liu Y, Zhang L, Mi HF, et al. The role of vitamin E in polyunsaturated fatty acid synthesis and alleviating endoplasmic reticulum stress in sub-adult grass carp (*Ctenopharyngodon idella*). Anim Nutr 2024;16:275–87.
Yao N, Feng L, Jiang W, Wu P, Ren H, Shi H, et al. An emerging role of arecoline on growth performance, intestinal digestion and absorption capacities and intestinal structural integrity of adult grass carp (*Ctenopharyngodon idella*). Anim Nutr 2023;15:173–86.
Yu E, Fu B, Wang G, Li Z, Ye D, Jiang Y, et al. Proteomic and metabolomic basis for improved textural quality in crisp grass carp (*Ctenopharyngodon idellus* C.et V) fed with a natural dietary pro-oxidant. Food Chem 2020;325:126906.
Yu YB, Li YQ. Enteric glial cells and their role in the intestinal epithelial barrier. World J Gastroenterol 2014;20(32):11273–80.
Zeng YY, Jiang WD, Liu Y, Wu P, Zhao J, Jiang J, et al. Dietary alpha-linolenic acid/linoleic acid ratios modulate intestinal immunity, tight junctions, anti-oxidant status and mRNA levels of NF-κB p65, MLCK and Nrf2 in juvenile grass carp (*Ctenopharyngodon idella*). Fish Shellfish Immunol 2016;51:351–64.
Zhang C, Hu QY, Feng L, Wu P, Liu Y, Kuang SY, et al. Isalo scorpion Cytotoxic peptide (IsCT) improved the physical barrier of the intestine on on-growing grass carp (*Ctenopharyngodon idella*). Aquaculture 2023;577:739895.
Zhang YL, Duan XD, Jiang WD, Feng L, Wu P, Liu Y, et al. Soybean glycinin decreased growth performance, impaired intestinal health, and amino acid absorption capacity of juvenile grass carp (*Ctenopharyngodon idella*). Fish Physiol Biochem 2019;45(5):1589–602.